Size effect in two-dimensional oxide-on-metal catalysts of CO oxidation and its connection to oxygen bonding: An experimental and theoretical approach

Ke Zhang,[#] Linfei Li, [#] Jacek Goniakowski,* Claudine Noguera

Hans-Joachim Freund, Shamil Shaikhutdinov*

[1] Department of Chemical Physics, Fritz Haber Institute of the Max Planck Society, Faradayweg 4-6, 14195 Berlin, Germany
[2] Institut des Nanosciences de Paris, 4 Place Jussieu, 75005 Paris, France

[#] These authors contributed equally to the work.

Corresponding authors: shaikhutdinov @fhi-berlin.mpg.de (S. Shaikhutdinov);
                            jacek.goniakowski@insp.jussieu.fr (J. Goniakowski)

Abstract

Transition metal oxide layers on metal surfaces often show superior catalytic performance as compared to conventional, i.e., metal-on-oxide, systems. In this work, we studied the CO oxidation reaction over FeO supported by Pt(111) and observed strong size effects on the reactivity. The monolayer islands below 5 nm in size showed a light-off temperature for CO_2 production 200 K lower than for the 30 nm islands. In an attempt to rationalize the size effect, we have performed oxygen desorption experiments and have combined them with an extended DFT analysis to provide insight into the bonding of various oxygen species in such systems. The theoretical results on isolated FeO_2 islands indicate a substantially lower stability of the boundary oxygen atoms as compared with the same islands embedded into an FeO layer in qualitative agreement with experiment showing that the smaller the island, the lower the desorption temperature. To the best of our knowledge, the results demonstrate the first example of a size effect in oxidation catalysis on *two-dimensional* systems.

Keywords: CO oxidation; monolayer catalysts; iron oxide; metal/oxide interface.

[#] These authors contributed equally to the work.

1. Introduction

Transition metal oxides (TMO) are active players in catalysis, in particular in oxidation reactions. The differentiation of the various oxygen species in activity is important and, therefore, needs speciation. This concept has been propagated prominently by Robert Grasselli [1, 2] with respect to oxidation of hydrocarbons on complex oxides, as well as by Jerzy Haber combining theory and experiment.[3-5] Even in the case of supported metal catalysts, where the noble metal particles are supported on a TM-oxide, the role of the oxide support often extends beyond that of being solely a template to fix the metal component, in that it actively participates in the process. A notable special case is represented by the so-called "Strong Metal Support Interaction" (SMSI), where the metal oxide may overgrow the supported metal particle and thus affect catalytic performance.[6] A detailed understanding of SMSI, whether it involves structural and/or electronic effects, remains under debate.[4, 7-10] SMSI often manifests itself *via* encapsulation of metal nanoparticles by a very thin oxide film stemming from a TMO support. Therefore, establishing the structure-reactivity relationships for *ultrathin* TMO films on metals may shed light on the SMSI effects.[11] In particular, the nature of oxygen species in the TMO films and its role in the oxidation reactions need to be better understood.

The interest in such studies increased after a "monolayer" FeO(111) film on Pt(111) was found to be active in low temperature CO oxidation, [12] and this is the film that encapsulates Pt nanoparticles supported on Fe_3O_4 as result of SMSI.[13, 14] However, under reaction conditions at near atmospheric pressures, the FeO(111) film transforms into the "O-rich" film with a compositional stoichiometry close to FeO_2 (henceforth referred to as a FeO_{2-x} film). Due to the Moiré-like coincidence structure formed on the initial FeO(111)/Pt(111) surface,[15] the O-rich film has a complex structure. Based on scanning tunneling microscopy (STM) studies [12] and density functional theory (DFT) calculations [16, 17], the film forms close-packed O-Fe-O trilayer islands, following the Moiré pattern, with an ill-defined structure between the islands. Temperature

programmed desorption (TPD) measurements showed that the FeO_{2-x} films contain oxygen species desorbing at much lower temperatures than in FeO. Weakly bound oxygen (WBO) species were attributed to the O atoms in the topmost layer. Accordingly, it is this oxygen that reacts with CO to form CO_2. Comparison with other TMO films tested in this reaction suggested that the binding energy of WBO species, determined by TPD, may serve as a descriptor for this reaction.[18]

At sub-monolayer oxide coverages, the oxide/metal interface starts to dominate the reactivity. Indeed, the CO_2 production rate increases and apparently follows the total island perimeter length, both reaching a maximum at mid-coverages.[19, 20] It was reasonably thought that CO strongly adsorbing on Pt reacts with the O atoms at the oxide island edge, either on the FeO/Pt [21] or FeO_2/Pt,[19] depending on reaction conditions. However, a more recent study [22] provided evidence for the steady state reaction taking place neither on FeO/Pt nor FeO_2/Pt interfaces, but at the boundary between oxidized and reduced phases of the iron oxide film formed under reaction conditions. In this scenario, the metal (Pt) surface solely aids in the initial formation of such boundaries close to the island edges rather than directly participates in the reaction.

In this work, we report substantial size effects of FeO islands on the CO oxidation reaction. Reducing the island size down to 5 nm considerably lowers the light-off temperature for CO_2 production. In an attempt to rationalize this effect, we have performed oxygen desorption experiments and have combined them with an extended DFT analysis to provide insight into the bonding of various oxygen species on such systems. The theoretical results on isolated FeO_2 islands indicate a substantially lower stability of the boundary oxygen atoms as compared with the same islands embedded into an FeO layer in qualitative agreement with experiment showing that the smaller the island, the lower the desorption temperature. To the best of our knowledge, the results demonstrate the first example of a size effect in oxidation catalysis on *two-dimensional* systems.

2. Methods and Materials

2.1 Experimental Section

The experiments were carried out in several UHV chambers (base pressures below 5×10^{-10} mbar) all equipped with standard facilities for cleaning the Pt(111) single crystal surface and preparation of the FeO(111) films. *In situ* STM studies were performed using a variable-temperature scanning tunneling microscope (VT-STM, Omicron). Temperature programmed reaction (TPR) measurements were performed in another chamber using a quadrupole mass-spectrometer (QMS, from Pfeiffer). The prepared samples were characterized with Omicron VT-STM/AFM at room temperature. Oxygen desorption experiments were performed in the third UHV chamber equipped with STM (Omicron) and QMS (Hiden).

In all setups, Fe was deposited using e-beam assisted evaporator (Focus EMT3) from an Fe rod (99.9999%, Sigma Aldrich). FeO(111) islands were prepared by Fe deposition onto a clean Pt(111) substrate in 10^{-7} mbar of O_2 at room temperature, followed by annealing in 10^{-6} mbar O_2 at 700 K for 5 min. In order to prepare the smallest FeO(111) islands, Fe was deposited onto a substrate kept at 100 K. The samples were then oxidized in 10^{-5} mbar O_2 at 573 K to transform FeO(111) into the FeO_{2-x} phase.

Computational Methods

All DFT calculations were performed with the Vienna Ab-initio Simulation Package (VASP),[23, 24] using Projector Augmented Wave (PAW) method [25, 26] to represent the electron-core interaction, and the Perdew-Wang 91 (PW91) [27] gradient-corrected exchange-correlation functional. Following our previous studies,[28, 29] iron oxides were treated with the DFT+U approach in the form proposed by Dudarev,[30] with $U_{Fe} - J_{Fe} = 3$ eV. FeO_X/Pt(111) system was represented by a three-layer-thick Pt(111) slab with the FeO_X oxide adsorbed on one side only. The bottom Pt layer was hold fixed while the two surface Pt layers and the oxide film were fully relaxed (threshold on forces equal to 0.01 eV/Å). The slabs were separated by at least 10 Å of vacuum and the dipole corrections were

applied in order to eliminate the residual dipoles in the direction perpendicular to the surface. In order to take into account the effect of lattice mismatch between the Pt(111) substrate and the oxide layer and to mimic the coincidence structures observed experimentally,[31] a ($\sqrt{73} \times \sqrt{73}$)R5.8°-FeO(111)//($\sqrt{91} \times \sqrt{91}$)R5.2°-Pt(111) periodic supercell has been used. Its large size makes Γ point sufficient to sample the Brillouin zone. Following our previous studies, soft oxygen pseudopotential (energy cutoff of 280 eV) was used and a row-wise anti-ferromagnetic alignment of Fe spins was systematically imposed. [19, 32] Atomic charges were estimated with the partition scheme proposed by Bader, [33, 34] and atomic configurations were plotted with VESTA.[35]

3. Results and Discussion

Experimental results

We first show how CO interacts with the FeO_{2-x} islands using *in situ* STM. Figure 1 displays STM images continuously recorded in 10^{-6} mbar of CO at 350 K for different exposure time as indicated. Regular protrusions imaged on the island surface reflect O-Fe-O trilayer domains showing the same periodicity (2.5 nm) as the Moiré structure in the original FeO(111)/Pt(111) films. Obviously, the reaction starts at the edge and propagates towards the center of the island until all FeO_2 related protrusions disappear due to their reduction back to FeO layer. Although STM tip effects cannot be ruled out, the reduced surface does not look atomically flat because the temperature (350 K) may not be high enough for complete structural relaxations accompanying the oxide reduction. Interestingly, the time required for CO to reduce FeO_2 domains at the perimeter is considerably shorter than that obtained for reduction of the next "spots ring" left (about 20 and 70 min, respectively). This finding suggests that the FeO_2 domains close to the island edge are much more reactive to CO than those located in the interior region of the island upon reaction front propagation. Henceforth, we referred to those as the "edge" and the "interior" spots, respectively.

5

Not surprisingly, the observed reaction is a thermally activated process. It proceeds much faster at increasing temperature. In order to get an estimate for the activation barrier, we imaged identically prepared samples all exposed to 10^{-6} mbar CO at several different temperatures between 300 and 450 K. In a crude approximation, we assume that the reaction rate is inversely proportional to the time (τ) needed for depleting the "edge" FeO_2 spots. The rate *vs* temperature dependence showed Arrhenius-like behavior (Figure 1), from which we calculated the apparent activation energy of ~40 kJ/mol. The energy barrier can be assigned to the CO + O -> CO_2 reaction step, which is considered as the rate-limiting step in the CO oxidation reactions following Mars-van Krevelen type mechanism.
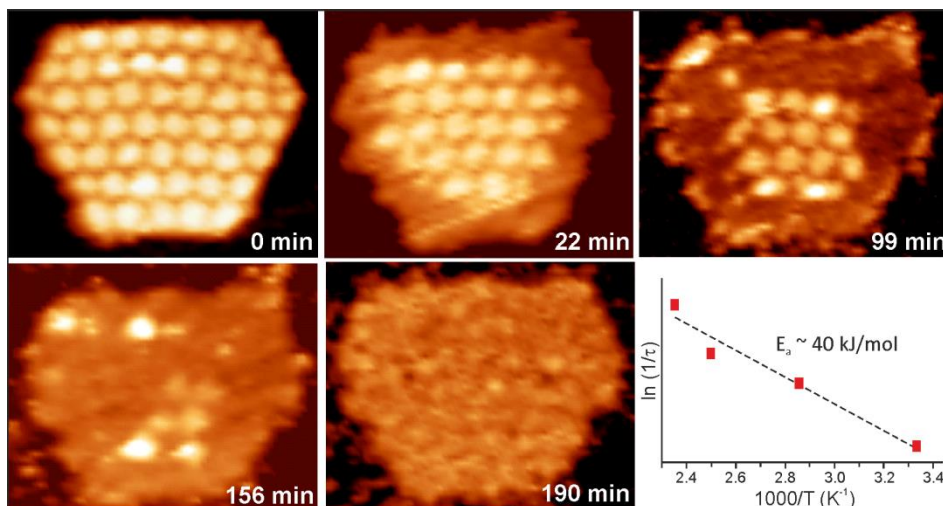

Figure 1. *In situ* STM images of an individual FeO_{2-x} island recorded in 10^{-6} mbar of CO at 350 K. Exposure time is indicated. (The image size is 24 nm × 20 nm; tunneling parameters: -2 V, 0.1 nA.) The panel shows the Arrhenius plot for the initial rate of reduction (measured by STM *ex situ*) as a function of temperature (300 - 450 K).

This high reactivity of FeO_2 spots at the island edge further manifested itself in the temperature programmed reduction (TPR) experiments summarized in Figure 2. Upon heating a sample in 10^{-6} mbar of CO, the latter reduces FeO_{2-x} to FeO producing CO_2 that has been recorded by a mass-spectrometer. The sample (1) has been prepared in such a way that it primarily exposes islands containing only "edge" spots as shown in the corresponding STM image. The maximum in CO_2 production on this sample is observed at

375 K. Then the sample was annealed in UHV at 650 K for 30 min to promote oxide sintering and re-oxidized in O_2 to transform islands back into the O-rich, FeO_{2-x} phase (sample 2) before the new TPR run. The procedure was repeated to prepare the samples (3) and (4). The morphology of each sample was inspected by STM before and after the TPR experiment.
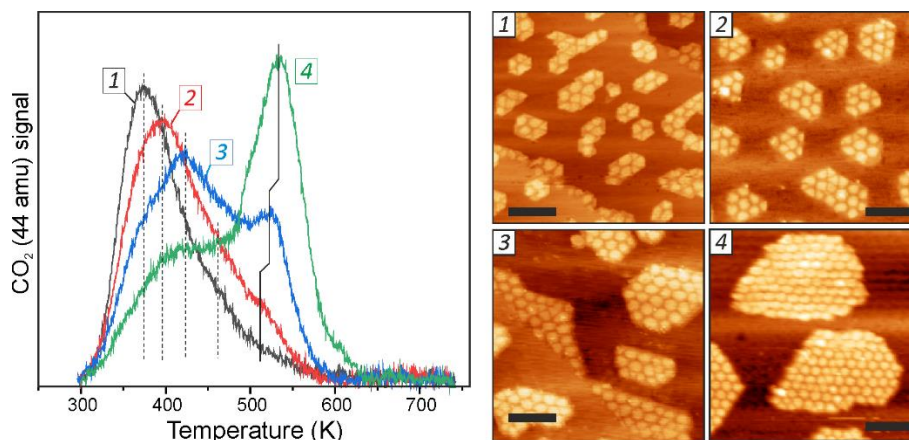

Figure 2. Temperature programmed reduction profiles measured on FeO_{2-x}/Pt(111) samples (1-4) shown in STM images (the scale bars are 10 nm) taken prior to the TPR run. The spectra are obtained by recording the CO_2 (44 amu) mass-spec signal in 10^{-6} mbar of CO upon linear heating with the rate 2 K/s.

It should be mentioned that the O ad-atoms remaining on the Pt(111) surface after sample preparation (exposure to 5×10^{-6} mbar O_2 at 573 K for 10 min, then pumping out and cooling to 300 K) readily react with residual CO in the UHV background during STM imaging and hence do not contribute to the CO_2 signal measured. Indeed, the four TPR spectra are very different, whereas the integral CO_2 signal area remains the same since the total oxide coverage is not changed upon islands sintering, but the island size.

TPR profiles revealed certain correlation with the sample morphology imaged by STM. It is clear that reaction at the lowest temperature occurs on the smallest islands exposing solely "edge" FeO_2 spots. As the island size increases, the total number of such spots decreases, and its contribution to overall CO_2 production diminishes. Concomitantly, the TPR profile shifts to higher temperatures, which is associated with the reaction propagating into the islands interior, as directly shown by *in situ* STM (Figure 1). Although

7

the low-temperature peak shifts to higher temperatures (from 375 to 420 K in samples (1)-(4), respectively), it seems to consist of several discrete components (indicated by dashed lines to guide the eye), each associated with the certain island size. Meanwhile a high-temperature signal is represented by one peak, albeit slightly shifting (from 510 to 535 K) at increasing size. Therefore, the combined TPR and STM results point out a strong size effect on CO reaction with O in oxide: The smaller the islands, the lower the light-off temperature and hence the activation energy for CO_2 formation.

In an attempt to rationalize exceptional activity of the "edge" FeO_2 spots and assuming that the binding energy of WBO species remains the descriptor for CO oxidation on partially covered films as well, we studied oxygen desorption using TPD. Figure 3a shows TPD spectra measured on FeO_{2-x}/Pt(111) films of three different coverages, *i.e.*, 0.25 , 0.5 and 1 ML (the latter corresponds to a dense monolayer (ML) film), determined from STM images shown as insets. Negligible oxygen desorption was detected on the FeO-free Pt(111) sample under the same preparation conditions, most likely due to the reaction with CO in the UHV background. The presented spectra show solely oxygen evolution during thermal reduction of the oxidized FeO_{2-x} phase into FeO, which, in turn, decomposes at temperatures as high as 1200 K.[12] The spectra clearly show that: (i) the signal intensity is proportional to the oxide coverage; (ii) the entire desorption profile shifts to higher temperatures with increasing coverage and/or island size; (iii) the desorption signals are highly symmetric and almost identical in shape.
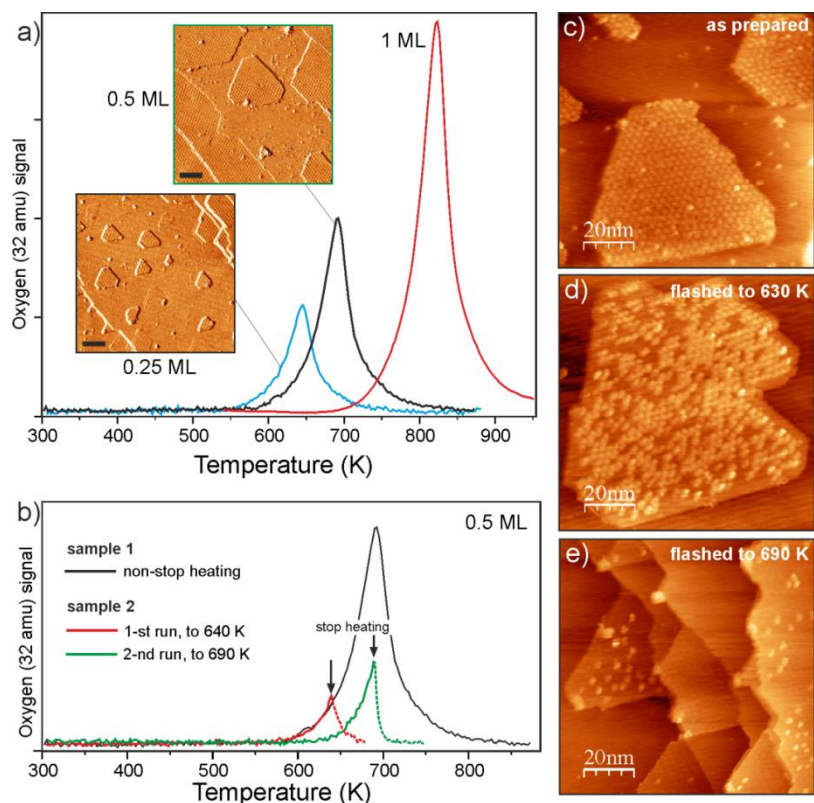
Figure 3. (a) O_2 (32 amu) TPD spectra recorded on FeO_{2-x}/Pt(111) at three different film coverages as indicated. STM images of the "as prepared" 0.25 and 0.5 ML samples (presented in the differentiated contrast) are shown in inset. The scale bar is 20 nm. (b) Black line reproduces the TPD spectrum for the 0.5 ML sample (1) from panel a). The newly prepared 0.5 ML sample (2) was first heated to 640 K (red line) and imaged with STM at 300 K. Then the sample was heated to 690 K (green line) and inspected by STM again. Dashed lines show (inertial) desorption traces after heating was stopped. The heating rate in all spectra is 2 K/s. (c-e) STM images of the sample "as prepared" (c) and after heating to 640 K (d) and 690 K (e), respectively.

It is interesting, that such spectra resemble those previously reported for noble metal surfaces oxidized at strongly oxidizing conditions and often referred to as "explosive" desorption.[36-38] In particular on Pt(111), the desorption peak was found to shift from 700 K to 750 on increasing nominal O coverage from 1.5 ML to 2.9 ML, respectively.[37] Other values are reported in Ref. [36]: the peak shifts from 680 K at 1.8 ML to 710 K at 2.4 ML. In principle, desorption temperatures observed in Figure 3a fall in the range obtained on oxidized Pt(111) surfaces. The O_2 desorption spectra on Pt(111) were originally explained by considering the influence of surface tension on the decomposition rates of PtO_x oxide particles presumably covering the surface.[36] As

particles increase in size, the rate at a given temperature decreases because the surface tension on the particles also decreases. Accordingly, the maximum desorption rate shifts to higher temperatures at increasing coverage. "Explosive" desorption occurs because as the particles shrink during decomposition they become increasingly less stable and hence decompose rapidly during the TPD experiments.

Such TPD behavior was later explained by a kinetic model in which O atoms migrate from oxide domains ("condensed phase") onto the surface regions containing chemisorbed oxygen atoms ("dilute phase").[37, 38] Desorption directly from the dense phase was considered to be negligible, and it preferentially occurred from the dilute phase, with the oxide islands and particles acting as a reservoir for O. The migration of species from the dense phase to the dilute phase was assumed to be faster than the desorption from either phase. Under these conditions, the desorption rate is proportional to the fraction of the surface covered by the dilute phase. Since this fraction increases as the dense phase is consumed, desorption is self-accelerating and the rate increases rapidly once desorption is initiated. Basically, explosive desorption occurs because the area of the surface from which species desorb, and hence the total desorption rate, increases until the dense phase is completely decomposed.

The latter mechanism seems hardly plausible for the case of FeO/Pt. First, on noble metal surfaces considered above, surface oxide domains (or particles) are fully reduced to the metal which is incorporated back to the metal surface. In our case, FeO_{2-x} islands only undergo reduction to FeO and do not vanish, thus the area of dilute phase remains constant. Second, the O atoms have to migrate across the FeO_x island to reach the perimeter. This step is not included in the above model, and no experimental results exist thus far to get an estimate for diffusion coefficients. Third, the amount of oxygen released during the FeO_{2-x} -> FeO transformation is, at most, 0.8 ML with respect to Pt(111).[12] Once all these O atoms spread onto the clean Pt(111) surface surrounding oxide islands covering 25% of the surface (the 0.25 ML sample, see Figure 3a), the amount of O ad-atoms would only be sufficient to form a (2×2)-O ad-layer which normally desorbs at about 750 K, *i.e.*, considerably higher than 640 K observed on this sample. In addition, the

kinetic model assumes (2×2)-O as the critical O concentration for the dilute phase, that must be *sustained via* dissolution of oxide phase.

To gain more insight into oxygen desorption from our films, we studied morphology of the 0.5 ML sample by STM after heating was stopped at 640 K, *i.e.*, shortly after the O_2 desorption starts. In the next run, the sample was heated to 690 K, that is the maximum desorption temperature, and again inspected by STM. Desorption traces are shown in Figure 3b together with the one obtained by non-stop heating to 900 K (replotted from Figure 3a) for direct comparison.

At first glance, comparison of STM images before and after heating to 640 K (Figure 3c,d) shows rather random disappearance of the FeO_2 spots due to their local thermal reduction to FeO. However, a closer look reveals that all "edge" spots have already disappeared at this point, clearly indicating preferential desorption from the islands edges that dominates in the initial stage of thermal reduction. During the next heating to 690 K, desorption only starts at the end temperature of the previous heating, *i.e.*, 640 K (Figure 3b). The leading edge basically follows the one observed in this temperature range in the "non-stop heated" TPD spectrum as if the desorption process continued from the surface formed in the previous run. After the sample was heated to 690 K, a small amount of FeO_2 spots remains on the islands (Figure 3e), which fully disappear after further heating to 900 K (not shown), ultimately recovering the FeO(111) surface. Therefore, STM results show that O_2 desorption starts within the FeO_2 spots at the island edge and then takes place randomly in the island interior.

In principle, the observed random desorption favors the mechanism of thermal reduction *via* O_2 desorption from oxide directly into the gas phase rather than *via* spillover of the O atoms onto the Pt surface from which they desorb associatively. Indeed, the desorption peak obtained for a dense film (*i.e.*, no Pt exposed) has the same shape as the partially covered samples do. In such scenario (desorption into the gas phase), the shift to lower temperatures at decreasing film coverage (Figure 3a) could be interpreted as if oxygen atoms in smaller FeO_{2-x} islands were more weakly bound. In this respect, we note a recent STM study [39] showing that FeO islands below 3 nm in size are more resistant

towards oxidation. This implies that "extra" O species in such small islands are less stable, and, therefore, the islands will more easily release oxygen during heating and thermal reduction. One may argue, that oxide islands studied here (tens of nanometers) are too large for invoking such a strong size effect. If the effect had a purely kinetic origin (larger island needs more time for oxygen desorption, thus causing the peak shifting to higher temperatures), then the TPD spectra would exhibit zero order kinetics with the same leading edge irrespective of the island size, at variance with the experiment. As a hypothesis, we could propose that oxygen desorption is affected by the size-dependent strain in the film as a result of a large (~ 10%) lattice mismatch between the oxide layer and metal surface. Indeed, looking at STM images one may notice that larger islands exhibit roundish and well-ordered FeO_2 spots, whereas such spots in the smallest islands as well as at the edge of large islands are considerably distorted.

Theoretical results

To get more insight into the oxygen stability in O-rich islands, we have performed DFT calculations on two models: FeO-embedded islands (Figure 4a) and isolated FeO_2 islands (Figure 4b). While the former describes the inner part of relatively large islands, the latter corresponds to the smallest, *i.e.*, single-spot island, but may also mimic the edge spots in larger islands.

The embedded model was obtained from the continuous FeO_2 tri-layer film by the removal of the most weakly bound oxygen atoms (see Sec. S1 in the Supporting Information, SI), as to preserve large uniform and well-structured tri-layer FeO_2 islands in registry with the Pt substrate, and a continuous FeO(111) lattice in between. Since the precise structure of these islands is yet unknown, we have purposely included both zig-zag- and arm-chair-oriented FeO_2/FeO boundaries. To allow a direct comparison, the isolated FeO_2 islands were constructed with the same stoichiometry, morphology, atomic structure, and position with respect to the substrate as the embedded ones.
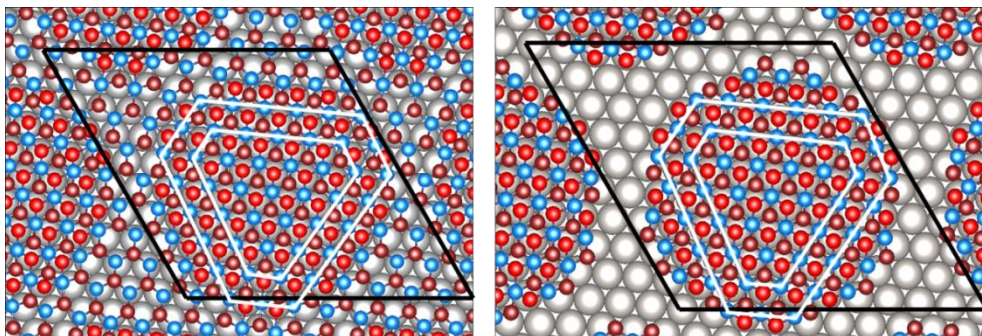
Figure 4. Models of FeO-embedded (a) and isolated (b) FeO$_2$ islands on the Pt(111) surface. Pt, Fe, and O atoms are represented by gray, blue, and red (light for interface, dark for surface) spheres, respectively. The peripheric, intermediate, and center zones of the FeO$_2$ islands are delimited (white lines) and the periodic ($\sqrt{73}\times\sqrt{73}$)R5.8°-FeO(111)//($\sqrt{91}\times\sqrt{91}$)R5.2°-Pt(111) unit cell is indicated (black lines).

In both models, the calculated individual oxygen vacancy formation energies (ΔE) tend to be systematically smaller for interface oxygen atoms and are by far the smallest for interfacial oxygen atoms at the island periphery (Secs. S2 and S3 in SI). This points toward a sequential desorption mode, which starts at the periphery of the FeO$_2$ islands and shifts progressively toward their centers. As a consequence, individual desorption energies are not fully representative of the actual energy cost of island reduction. They also neglect the collective effects in desorption of O$_2$ molecules. To better approximate the desorption thermodynamics, we have simulated the desorption process by the stepwise collective removal of interfacial oxygen atoms successively in the three regions (delimited by white lines in Figure 4), starting from the island periphery. After each desorption stage, the size of the FeO$_2$ region decreases, and the FeO/FeO$_2$ boundary shifts toward the island center.

Table 1 reports the average desorption energies ($\Delta\varepsilon$) at each stage. The lower values of $\Delta\varepsilon$ compared to the average of individual values ΔE for the atoms upon consideration (Secs. S2 and S3 in SI) highlight the importance of collective effects in the desorption process. Moreover, contrary to an average of all ΔE values, the average of the three $\Delta\varepsilon$ values reproduces very well the total energy cost (per atom) of a full island reduction (simultaneous removal of all 54 interfacial oxygen atoms in the model), equal to 1.08 eV and 1.01 eV per atom for the embedded and isolated islands, respectively. This difference

corresponds to a nearly 4 eV larger energy cost of the full reduction of the embedded island.

Table 1. Average vacancy formation energies $\Delta\varepsilon$ (eV/atom) for the stepwise removal of oxygen atoms in embedded and isolated FeO$_2$ islands. Each successive stage corresponds to the desorption of 18 interfacial oxygen atoms from the peripheric, intermediate, and inner regions, respectively, as shown in Figure 4.

$\Delta\varepsilon$ (eV/atom)	Stage I (Peripheric)	Stage II (Intermediate)	Stage III (Inner)
Embedded island	0.95	1.13	1.15
Isolated island	0.95	1.06	0.99

Calculated $\Delta\varepsilon$ values show that oxygen stabilities in the two types of island differ quite considerably. While the difference in $\Delta\varepsilon$ is marginal at the first stage I, it becomes significant at the stage II (0.07 eV/atom), and substantial at stage III (0.16 eV/atom). Moreover, for the embedded islands, the increase of $\Delta\varepsilon$ when moving towards the island center suggests a slowdown of oxygen desorption, whereas such effect is not obvious for the isolated islands. The systematically lower oxygen stability in the isolated islands and the enhanced stability of inner oxygen atoms in the embedded ones are qualitatively consistent with the measured lower oxygen desorption temperature from smaller islands and to the observed greater facility to desorb oxygen atoms from the edges of large islands. This finding may also explain the *in situ* STM results (Figure 1), showing considerable increase of the time required for CO to reduce FeO$_2$ domains during the propagation of the reaction towards the island center.

To rationalize the origin of the differences between $\Delta\varepsilon$ values for the isolated and embedded islands, we compared the evolution of their structural characteristics as a function of island size. Synthetic, spatially-resolved information on the oxide structure is provided by the average Fe-Fe distances around cations along the unit cell long diagonal

(see Figure 4). Figure 5 shows that, while the initial Fe-Fe distances in the embedded and isolated FeO_2 islands display similarities (compare black lines), their behavior upon progressive oxygen desorption differs significantly, thus suggesting that strain release effects play a role in the different oxygen stability in the two types of islands.
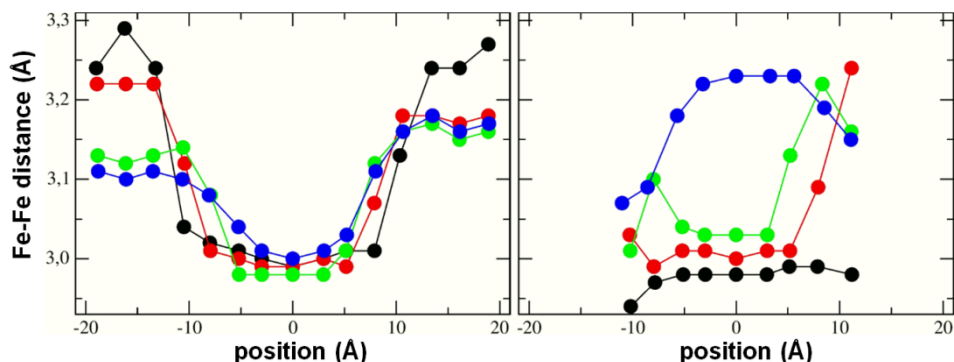

Figure 5. Local average values of Fe-Fe distances (Å) for cations along the cell long diagonal for the embedded (left) and isolated (right) islands: initial FeO_2 (black); with peripheric O atoms desorbed (red); with peripheric and intermediate O atoms desorbed (green); and fully reduced FeO (blue) islands. (For atomic representations of islands at the various stages of reduction see Figure S6 in SI.)

In the embedded case, the Fe-Fe distances in the interior of the FeO_2 islands are nearly size independent and only slightly differ from those in the pristine FeO film in the same region of the Moiré cell. Thus, the embedded O-rich region is not subject to a substantial strain release upon oxygen desorption. However, the structure of the FeO film between the FeO_2 islands undergoes important modifications. Indeed, short in-plane lattice parameters of FeO_2, consistent with a strong oxide-metal interaction and a large rumpling in the O-Fe-O trilayer film, induce a tensile strain in the inter-island FeO layer. This strain is particularly strong around the full FeO_2 islands (black lines in Figure 5), where it produces the largest expansion of the Fe-Fe distances in the FeO zone with respect to those in the corresponding pristine FeO layer (blue). Unsurprisingly, the effect diminishes upon removal of peripheric O atoms (red) and becomes quasi-negligible in the smallest embedded islands (green). In order to estimate the consequence of such strain release on oxygen desorption, in a separate calculation we have released the strain of the FeO region by removing four oxygen atoms from its center. We found that it results in an

increase of $\Delta\varepsilon$ at the stage I by as much as 0.1 eV/atom (Sec. S3 in SI). We thus conclude that the strong tensile strain in the embedding FeO regions substantially reduces the binding of the peripheric O atoms and somewhat weakens the binding of the intermediate ones. It, therefore, explains the progressive increase of $\Delta\varepsilon$ at the subsequent stages of oxygen desorption from the embedded FeO_2 islands (Table 1).

In the isolated island, the Fe-Fe distances in the full FeO_2 islands (black), are fairly similar to those in the embedded one, suggesting that $d_{Fe-Fe} \approx 3.0$ Å represents the in-plane lattice parameter in the FeO_2/Pt(111) nano-oxide. However, in stark contrast with the embedded case, these distances are much shorter than those in the corresponding fully reduced island (blue). As a consequence, at the successive stages of oxygen desorption, the progressive increase of size of the FeO boundary induces a progressive expansion of the Fe-Fe distances within the remaining FeO_2 region. Such behavior indicates the presence of a tensile strain in the FeO_2 region, induced by the FeO border. The effect is clearly the most pronounced at the stage III of desorption, at which the departure of oxygen atoms additionally enables a thorough relaxation of the entire FeO island which is additionally accompanied by a change of its registry with respect to the Pt(111) surface. In direct analogy with the embedded case, the presence of such FeO-induced tensile strain reduces the strength of oxygen binding in the FeO_2 region, is responsible for the systematically lower $\Delta\varepsilon$ values in the isolated case, and explains the significant reduction of $\Delta\varepsilon$ for the inner oxygen atoms.

To summarize, calculations reveal the specific character of the FeO_2/FeO boundary: a large stability difference between surface and interface oxygen atoms and a substantial binding reduction of the latter. As a consequence, oxygen desorption is likely a sequential process triggered by oxygen binding reduction at the progressing FeO_2/FeO boundary. Moreover, while different ion coordination and Fe-O bond iono-covalency contribute to the stability of boundary oxygen atoms, we show that strain also plays a prominent role. Indeed, the non-negligible difference of in-plane lattice parameters in the oxygen-rich and oxygen-poor regions affects the oxygen stability at the edges of the embedded islands *via* a strong tensile strain in the inter-island FeO region. Conversely, the tensile strain

16

induced by the reduced border is the robust cause of oxygen destabilization in the isolated island.

These computational results are consistent with the size effect observed experimentally and clearly show that the thermodynamic stability of oxygen in the FeO_2 nano-oxide is sensitive to both its direct environment and to the size of the oxygen-rich phase. However, a translation of the calculated desorption energies $\Delta\varepsilon$ into desorption temperatures using a Redhead analysis as in Ref. [19] leads to differences between embedded and isolated islands roughly twice smaller than those measured experimentally. Several effects of different nature may contribute to such an underestimation. On the one hand, regarding the thermodynamics of desorption, the computational models remain somewhat arbitrary. In particular, while the actual state of the embedding inter-island FeO region under desorption conditions is unknown, we have shown that its strain state significantly affects oxygen stability at the FeO/FeO_2 boundary. Interestingly, the roughness of the FeO layer directly after oxygen desorption visible in the STM images (Figure 1) points toward a partial release of the tensile strain in the embedding film. According to our theoretical analysis, this should produce an additional stabilization of oxygen at boundaries of embedded islands, and thus bring the theoretical estimation closer to the measurements. On the other hand, regarding kinetics of oxygen desorption from the boundaries, it may involve activation barriers which do not scale linearly with energy of oxygen desorption, as assumed in Ref.[19] An explicit account for energy barriers associated with alternative oxygen recombination and desorption pathways would be necessary to refine the present thermodynamics-driven estimation.

4. Conclusions

Our experimental results show that the CO oxidation reaction on FeO monolayer islands supported by Pt(111) primarily occurs on FeO/FeO_2 interface formed under reaction conditions along the islands edge which can be considered as a dynamically fluctuating "reaction zone". Its width (~ 3 nm) is comparable with the size of a Moiré unit

cell in epitaxial FeO(111)/Pt(111) films thus suggesting the peculiar reactivity of the oxide in the "edge" zone, whereas well-ordered interior regions are relatively inert. As a result, reactivity strongly depends on island size. The islands only consisting of the edge reaction zone show considerably lower (by about 200 K) CO_2 formation temperature than the extended islands.

In an attempt to rationalize this effect, we performed oxygen desorption experiments and combined them with an extended DFT analysis to provide insight into the bonding of various oxygen species in such systems since O binding energy has been found as a good descriptor for this reaction on the dense monolayer oxide films. The theoretical results on isolated FeO_2 islands indicate a substantially lower stability of the boundary oxygen atoms as compared with the same islands embedded into an FeO layer in qualitative agreement with TPD results showing that the smaller the island, the lower the oxygen desorption temperature.

Size effects are well documented in catalysis over highly dispersed metals in structure sensitive reactions, which are commonly rationalized in terms of abundance of under-coordinated surface atoms on smaller particles considered as the most active sites. Herein, the effect is observed on the *two-dimensional* system.

It should be mentioned that TMO deposits on metal substrates have been long considered as model "inverse" catalysts [40] for studying chemical reactions at the interface between the metal particle and oxide support in "conventional" metal-on-oxide catalysts. Since TMO deposits often form monolayer islands rather than spherical particles,[41] the coverage effects reported for "inverse" model catalysts may be affected by the island size and even cause some discrepancy, if the islands size is not controlled or directly measured.

References

[1] R.K. Grasselli, Selective Oxidation and Ammoxidation Catalysis: Mechanism and Commercial Practice, in: J.P. Bonnelle, B. Delmon, E. Derouane (Eds.) Surface Properties and Catalysis by Non-Metals, Springer Netherlands, Dordrecht, 1983, pp. 289-304.

[2] R.K. Grasselli, Fundamental Principles of Selective Heterogeneous Oxidation Catalysis, Topics in Catalysis, 21 (2002) 79-88.

[3] A. Bielański, J. Haber, Oxygen in Catalysis on Transition Metal Oxides, Catalysis Reviews, 19 (1979) 1-41.

[4] J. Haber, M. Witko, Oxidation catalysis—electronic theory revisited, Journal of Catalysis, 216 (2003) 416-424.

[5] J. Haber, Catalytic Oxidation -State of The Art and Prospects, in: P. Ruiz, B. Delmon (Eds.) Studies in Surface Science and Catalysis, Elsevier, 1992, pp. 279-304.

[6] S.J. Tauster, Strong metal-support interactions, Accounts of Chemical Research, 20 (1987) 389-394.

[7] F. Solymosi, Importance of the Electric Properties of Supports in the Carrier Effect, Catalysis Reviews, 1 (1968) 233-255.

[8] G.L. Haller, D.E. Resasco, Metal–Support Interaction: Group VIII Metals and Reducible Oxides, in: H.P. D.D. Eley, B.W. Paul (Eds.) Adv. Catal., Academic Press, 1989, pp. 173-235.

[9] S. Bernal, J.J. Calvino, M.A. Cauqui, J.M. Gatica, C. Larese, J.A. Pérez Omil, J.M. Pintado, Some recent results on metal/support interaction effects in NM/CeO2 (NM: noble metal) catalysts, Catalysis Today, 50 (1999) 175-206.

[10] F.F. Vol'kenshtein, Experiment and the electronic theory of catalysis, Russian Chemical Reviews, 35 (1966) 537.

[11] S. Shaikhutdinov, Strong Metal–Support Interaction and Reactivity of Ultrathin Oxide Films, Catalysis Letters, 148 (2018) 2627-2635.

[12] Y.-N. Sun, L. Giordano, J. Goniakowski, M. Lewandowski, Z.-H. Qin, C. Noguera, S. Shaikhutdinov, G. Pacchioni, H.-J. Freund, The Interplay between Structure and CO Oxidation Catalysis on Metal-Supported Ultrathin Oxide Films, Angewandte Chemie International Edition, 49 (2010) 4418-4421.

[13] Z.H. Qin, M. Lewandowski, Y.N. Sun, S. Shaikhutdinov, H.J. Freund, Encapsulation of Pt Nanoparticles as a Result of Strong Metal−Support Interaction with Fe3O4(111), The Journal of Physical Chemistry C, 112 (2008) 10209-10213.

[14] M.G. Willinger, W. Zhang, O. Bondarchuk, S. Shaikhutdinov, H.-J. Freund, R. Schlögl, A Case of Strong Metal–Support Interactions: Combining Advanced Microscopy and Model Systems to Elucidate the Atomic Structure of Interfaces, Angewandte Chemie International Edition, 53 (2014) 5998-6001.

[15] G.H. Vurens, V. Maurice, M. Salmeron, G.A. Somorjai, Growth, structure and chemical properties of FeO overlayers on Pt(100) and Pt(111), Surface Science, 268 (1992) 170-178.

[16] L. Giordano, M. Lewandowski, I.M.N. Groot, Y.N. Sun, J. Goniakowski, C. Noguera, S. Shaikhutdinov, G. Pacchioni, H.J. Freund, Oxygen-Induced Transformations of an FeO(111) Film on Pt(111): A Combined DFT and STM Study, Journal of Physical Chemistry C, 114 (2010) 21504-21509.

[17] L.R. Merte, Y. Bai, H. Zeuthen, G. Peng, L. Lammich, F. Besenbacher, M. Mavrikakis, S. Wendt, Identification of O-rich structures on platinum(111)-supported ultrathin iron oxide films, Surface Science, 652 (2016) 261-268.

[18] Y. Martynova, S. Shaikhutdinov, H.-J. Freund, CO Oxidation on Metal-Supported Ultrathin Oxide Films: What Makes Them Active?, Chemcatchem, 5 (2013) 2162-2166.

[19] Q. Pan, X. Weng, M. Chen, L. Giordano, G. Pacchioni, C. Noguera, J. Goniakowski, S. Shaikhutdinov, H.-J. Freund, Enhanced CO Oxidation on the Oxide/Metal Interface: From Ultra-High Vacuum to Near-Atmospheric Pressures, ChemCatChem, 7 (2015) 2620-2627.

[20] Y. Martynova, B.H. Liu, M.E. McBriarty, I.M.N. Groot, M.J. Bedzyk, S. Shaikhutdinov, H.J. Freund, CO oxidation over ZnO films on Pt(111) at near-atmospheric pressures, Journal of Catalysis, 301 (2013) 227-232.

[21] D. Sun, X.-K. Gu, R. Ouyang, H.-Y. Su, Q. Fu, X. Bao, W.-X. Li, Theoretical Study of the Role of a Metal–Cation Ensemble at the Oxide–Metal Boundary on CO Oxidation, The Journal of Physical Chemistry C, 116 (2012) 7491-7498.

[22] K. Zhang, L. Li, S. Shaikhutdinov, H.-J. Freund, Carbon Monoxide Oxidation on Metal-Supported Monolayer Oxide Films: Establishing Which Interface is Active, Angewandte Chemie International Edition, 57 (2018) 1261-1265.

[23] G. Kresse, J. Furthmüller, Efficient iterative schemes for ab initio total-energy calculations using a plane-wave basis set, Physical Review B, 54 (1996) 11169-11186.

[24] G. Kresse, J. Hafner, Ab initio molecular-dynamics simulation of the liquid-metal--amorphous-semiconductor transition in germanium, Physical Review B, 49 (1994) 14251-14269.

[25] G. Kresse, D. Joubert, From ultrasoft pseudopotentials to the projector augmented-wave method, Physical Review B, 59 (1999) 1758-1775.

[26] P.E. Blöchl, Projector augmented-wave method, Physical Review B, 50 (1994) 17953-17979.

[27] J.P. Perdew, J.A. Chevary, S.H. Vosko, K.A. Jackson, M.R. Pederson, D.J. Singh, C. Fiolhais, Atoms, molecules, solids, and surfaces: Applications of the generalized gradient approximation for exchange and correlation, Physical Review B, 46 (1992) 6671-6687.

[28] L. Giordano, G. Pacchioni, J. Goniakowski, N. Nilius, E.D.L. Rienks, H.-J. Freund, Interplay between structural, magnetic, and electronic properties in a FeO/Pt(111) ultrathin film, Physical Review B, 76 (2007) 075416.

[29] S. Prada, L. Giordano, G. Pacchioni, C. Noguera, J. Goniakowski, Properties of Pt-supported iron oxide ultra-thin films: Similarity of Hubbard-corrected and hybrid density functional theory description, The Journal of Chemical Physics, 141 (2014) 144702.

[30] S.L. Dudarev, G.A. Botton, S.Y. Savrasov, C.J. Humphreys, A.P. Sutton, Electron-energy-loss spectra and the structural stability of nickel oxide: An LSDA+U study, Physical Review B, 57 (1998) 1505-1509.

[31] M. Ritter, W. Ranke, W. Weiss, Growth and structure of ultrathin FeO films on Pt(111) studied by STM and LEED, Physical Review B, 57 (1998) 7240-7251.

[32] L. Giordano, G. Pacchioni, C. Noguera, J. Goniakowski, Identification of Active Sites in a Realistic Model of Strong Metal–Support Interaction Catalysts: The Case of Platinum (1 1 1)-Supported Iron Oxide Film, ChemCatChem, 6 (2014) 185-190.

[33] R.F.W. Bader, A quantum theory of molecular structure and its applications, Chemical Reviews, 91 (1991) 893-928.

[34] G. Henkelman, A. Arnaldsson, H. Jónsson, A fast and robust algorithm for Bader decomposition of charge density, Computational Materials Science, 36 (2006) 354-360.

[35] K. Momma, F. Izumi, VESTA 3 for three-dimensional visualization of crystal, volumetric and morphology data, Journal of Applied Crystallography, 44 (2011) 1272-1276.

[36] N.A. Saliba, Y.L. Tsai, C. Panja, B.E. Koel, Oxidation of Pt(111) by ozone (O3) under UHV conditions, Surface Science, 419 (1999) 79-88.

[37] J.F. Weaver, J.-J. Chen, A.L. Gerrard, Oxidation of Pt(111) by gas-phase oxygen atoms, Surface Science, 592 (2005) 83-103.

[38] B. Klötzer, K. Hayek, C. Konvicka, E. Lundgren, P. Varga, Oxygen-induced surface phase transformation of Pd(111): sticking, adsorption and desorption kinetics, Surface Science, 482-485 (2001) 237-242.

[39] Y. Liu, F. Yang, Y. Zhang, J. Xiao, L. Yu, Q. Liu, Y. Ning, Z. Zhou, H. Chen, W. Huang, P. Liu, X. Bao, Enhanced oxidation resistance of active nanostructures via dynamic size effect, Nature Communications, 8 (2017) 14459.

[40] K. Hayek, B. Jenewein, B. Klötzer, W. Reichl, Surface reactions on inverse model catalysts: CO adsorption and CO hydrogenation on vanadia- and ceria-modified surfaces of rhodium and palladium, Topics in Catalysis, 14 (2000) 25-33.

[41] F.P. Netzer, F. Allegretti, S. Surnev, Low-dimensional oxide nanostructures on metals: Hybrid systems with novel properties, Journal of Vacuum Science & Technology B: Microelectronics and Nanometer Structures, 28 (2010) 1-16.